Journal of Natural Gas Science and Engineering 52 (2018) 235–247

Contents lists available at ScienceDirect

Journal of Natural Gas Science and Engineering

journal homepage: www.elsevier.com/locate/jngse

A visualization study of proppant transport in foam fracturing fluids

Songyang Tong, Robin Singh, Kishore K. Mohanty*

Department of Petroleum and Geosystems Engineering, The University of Texas at Austin, 200 E. Dean Keeton, Austin, TX 78712, USA

ARTICLE INFO

Keywords:
Proppant transport
Settling velocity
Foam
Viscous fingering

ABSTRACT

The placement of proppants in hydraulically fractured wells determines the conductivity of fractures and the productivity of shale wells. In slickwater farcturing, proppants are often not transported deep into fractures. In this paper, proppant transport in foam-based fracturing fluid is visualized in a laboratory-scale fracture slot. Effect of parameters like foam quality, proppant loading, and injection rate are systematically investigated. Experiments show that dry foams (80% quality) can carry proppants between the lamellas with little vertical settling. A complex flow pattern develops at the bottom of the slots in dry foams due to protrusion of foam fingers into proppant laden foam flow. Proppants are not carried very well in wet foams (70% quality) and form a proppant bed near the injection well. This is due to drainage of liquid and low effective viscosity of the foam as it moves through the fracture.

1. Introduction

The commercial exploitation of unconventional shale has led to a dramatic increase in the production of oil and gas in the US. Slickwater (water mixed with a small amount of friction reducer) fracturing is commonly used because it produces a thin, long primary fracture intersecting secondary fractures. However, common proppants such as sand settle down very quickly in slickwater (Tong and Mohanty, 2016) and leave a large portion of fracture surfaces and network unpropped or sealed after stimulation (Kern et al., 1959; Mohanty et al., 2017; Warpinski et al., 2009; Yu et al., 2014), which could potentially leads to the underperformance of fracturing. There are two common methods to transport the proppants deep into the fractures. The first method is to use polymer-based viscous fracturing fluids. They carry the proppants well, but can plug the tiny pores in low permeability shales and damage the productivity of the fractures (Barati and Liang, 2014; Ribeiro and Sharma, 2012; Yang and Balhoff, 2017). Zhou et al. (2015) included guar-based polymeric particles in the fracturing fluid, and these particles could take the space between the proppants and prevent proppants from settling. After cleaning, no gel or filter cake damage was found, and the fracture could regain 91% of its conductivity. The second method is to use ultra-light weight proppants (ULWP) (Gaurav et al., 2012). ULWPs usually have a specific gravity of 1.08–2.0 (which lies between the specific gravity of water and sand). Based on Stoke's Law, ULPWs have significantly smaller settling velocity compared to that of sand. However, ULWPs typically offer a lower conductivity compared to conventional proppants (Rickards et al., 2006) and may suffer severe flowback issues.

Another alternative approach is to use foam fluids. Foams possess high apparent viscosity (Kong et al., 2016; McAndrew et al., 2017; Xu et al., 2017) which is good for suspending proppants. In addition, foams reduce water use, fracturing fluid leak-off, clay swelling and lead to faster fracture clean-up due to gas expansion (Gu and Mohanty, 2014). Foam fluid has been widely investigated by previous researchers (Reidenbach et al., 1986; Harris and Reidenbach, 1987; Harris, 1989, 1995). Temperature, pressure, gas types and additives determined the bubble property and foam stability. Foam stability at high temperature depended more on surfactant type and concentration (Harris and Reidenbach, 1987). Generally, a Herschel-Bulkley model or a power-law model was used to describe the rheological behavior of foams (Reidenbach et al., 1986), and the rheology was hardly affected by the type of gas (Harris, 1995).

Transparent Hele-Shaw slots have been widely used to visualize and investigate proppant transport in the literature (Liu and Sharma, 2005; Malhotra et al., 2014; Zhou et al., 2015). Liu and Sharma, 2005 systematically studied proppant settling within a rough-walled Hele-Shaw slot. Effect of fracture width, fluid rheology, proppant diameter and concentration were incorporated into an empirical settling velocity of concentrated proppant slurry. Malhotra et al. (2014) made use of viscous fingering phenomenon (Doorwar and Mohanty, 2011) and developed an alternate-slug pumping of polymeric fluid and just water to enhance proppant transport. Proppant could be nicely held in fingers generated by adverse viscosity fronts. Proppant transport in foams has not been visualized in Hele-Shaw slots.

In this work, proppant transport in foam has been investigated

* Corresponding author.
E-mail address: kishore.mohanty@engr.utexas.edu (K.K. Mohanty).

https://doi.org/10.1016/j.jngse.2018.01.030
Received 4 October 2017; Received in revised form 10 December 2017; Accepted 25 January 2018
Available online 31 January 2018
1875-5100/

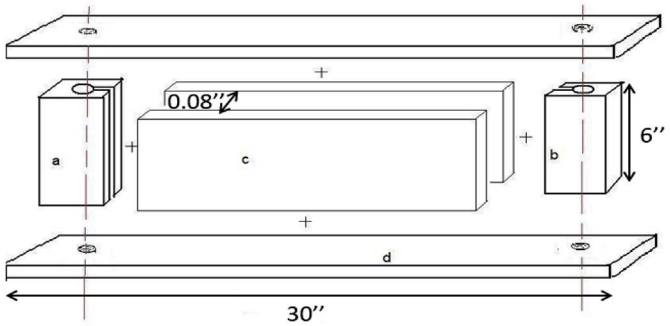

Fig. 1. Dimensions of the slot (hele-shaw slot) used in the study.

systematically at the room conditions. At the field conditions, the density of the gas can change considerably and would affect the liquid drainage; but that is outside the scope of this study. We conducted dynamic proppant settling experiments in foam within a transparent Hele-Shaw slot, and proppant trajectory was tracked. The effects of foam quality, proppant loading and injection rate on proppant velocity were analyzed with trajectories.

2. Methodology

2.1. Materials

A C14-16 alpha-olefin sulfonate (AOS) anionic surfactant (39% active) was used in this study. This surfactant is an effective foaming agent and has been reported in foam fracturing (Gu and Mohanty, 2015) and EOR studies (Singh and Mohanty, 2017). A partially (30%) hydrolyzed polyacrylamide polymer with a molecular weight of 8 million Dalton was added into the solution as a viscosifier. Sodium chloride was used as received. 20-40 mesh size black ceramic proppant (specific gravity: 3.36) was selected in this study for better visualization (Kadhim et al., 2017). The foam fluid was prepared with 0.5 wt% surfactant in 1.0 wt% NaCl brine with 100 ppm polymer. Foam rheology was quantified with a power-law model based on pipe rheometry measurements. Measurement details could be found elsewhere in the literature (Enzendorfer et al., 1995).

2.2. Fracture slot

A transparent Hele-Shaw slot was used to mimic hydraulic fractures, and it is 30″, 6″ and 0.08″ in length, height, and width, respectively. This slot was designed to visualize the process of proppant transport in foam. Fig. 1 shows the schematic figure of the slot design. The inlet is on the left, and the outlet is on the right. The inlet and outlet holes were 0.5″ in diameter which run along the height of the slot (components a and b in Fig. 1). Note that this diameter (0.5″) is very large as compared to the width of the slot (0.08”); therefore, the holes also act as a fluid distributor which minimizes the entrance effects. Both top and bottom plates were attached to the slot (unlike the figure). Foam-proppant slurry was mixed in a blender at a fixed rpm to form a homogeneous mixture of proppant-laden foam. This mixture was injected in the slot using a peristaltic pump running at a constant flow rate, as shown in Fig. 2. The movement of proppant was recorded with cameras, and the trajectory of proppant was tracked in a video analysis software. The bubble texture of the foam in the Hele-Shaw cell was characterized using a Nikon optical microscope equipped with a high-resolution camera. The image processing was done using the open-source Fiji software. The pressure drop across the cell was measured using a Rosemount differential pressure transducer.

2.3. Experimental conditions

Black-colored, 20/40 ceramic proppant was used for better visualization (compared to sand). Effects of proppant loading and shear rate were investigated. The concentration of proppant varied from 2.5 vol% to 10.0 vol% (around 0.6–2.4 ppg sand loading), which is within the range of typical field applications. Due to the limitation of the pump, the maximum injection velocity and corresponding shear rate were 0.0467 m/s and 140 s^{-1}, respectively. The nominal shear rate (γ) in a rectangular channel is defined as

$$\gamma = \frac{6q}{w^2 h} \quad (1)$$

where q is the volumetric flow rate in the channel, w is the width (the shorter dimension of the channel), and h is the height. This shear rate is not an actual local shear rate because the formation of proppant bed can significantly affect the flow of the fluid.

The experimental matrix is listed in Table 1. 80% quality foam was studied comprehensively, and several experiments were conducted with the 70% quality foam for comparison. Foam quality is defined as the volume percentage of gas in the foam. Experiments were performed at common shear rates observed in the field applications (Ouyang et al., 2012). Proppant loading is the volume% of proppant in the slurry. Equivalent Sand Loading (ESL) is the lbs of sand proppant per gallon of slurry if sand is used as the proppant at the same volume %. It is calculated by multiplying sand density (lb/gallon) and proppant volume concentration. ESL is another way to express proppant loading.

3. Results and discussion

3.1. Static foam test

Static foam tests (SFT) are one of the most common bulk foam stability experiments which are extensively used in the literature for screening foaming formulations (Andrianov et al., 2012; Singh and Mohanty, 2016; Vikingstad et al., 2005). In this study, SFT were conducted to investigate the effect of polymer and foam quality on the bulk foam stability. Static foam tests were conducted for 70% and 80% foam

Fig. 2. Experiment setup.

Table 1
Experimental matrix.

Case #	Foam quality	Nominal shear rate (1/s)	Nominal velocity (cm/s)	Proppant Loading (vol %)	ESL (ppg)
1	80%	42	1.39	2.5	0.6
2	80%	42	1.39	5.0	1.2
3	80%	42	1.39	7.5	1.8
4	80%	42	1.39	10.0	2.4
5	80%	84	2.78	2.5	0.6
6	80%	84	2.78	5.0	1.2
7	80%	84	2.78	7.5	1.8
8	80%	84	2.78	10.0	2.4
9	80%	140	4.67	2.5	0.6
10	80%	140	4.67	5.0	1.2
11	80%	140	4.67	7.5	1.8
12	80%	140	4.67	10.0	2.4
13	70%	42	1.39	2.5	0.6
14	70%	84	2.78	2.5	0.6
15	70%	140	4.67	2.5	0.6
16	70%	140	4.67	5.0	1.2
17	70%	140	4.67	7.5	1.8

with and without 100 ppm polymer. The decay of foam column height was monitored up to 48 h. These tests were performed at room condition. Fig. 3a shows the normalized foam height against the decay time in hours. Half-life, which is the time that the foam takes to decay to half of its original height, could be obtained from the figure. Fig. 3b shows the decay profile of the first 2 h, which is a timeframe of a typical fracturing application. There are two main foam destabilization mechanisms which govern the bulk foam stability: Ostwald ripening and liquid drainage in lamellae. The addition of polymer increases the viscosity of the liquid phases which reduces the rate of liquid drainage process. Fig. 3a shows that the foam decay profile for the cases of 80% foam with polymer is much slower than 80% foam without polymer, especially during late times (> 12 h) when foam lamellae are very thin.

3.2. Foam rheology

A pipe viscometer was used to quantify the foam rheology. The length (L) and inner diameter (d) of the pipe are 2 ft and 0.25 inch, respectively. Different injection rates were applied for different shear rates, and pressure drop (ΔP) was measured along the pipe. The apparent wall shear rate is calculated as

$$\gamma_{wa} = \frac{32q}{\pi d^3} \tag{2}$$

and the wall shear stress τ_w is calculated as

$$\tau_w = \frac{d\Delta P}{4L} \tag{3}$$

where q is the volumetric foam injection rate in the pipe. A power-law model was used in this study to describe the foam rheology:

$$\tau = K\gamma^n \tag{4}$$

where K is the consistency index and n is the flow behavior index. γ_{wa} should be converted to intrinsic shear rate γ_{wi} in Eq. (4) if τ is the wall shear stress τ_w (Enzendorfer et al., 1995). The conversion could be done as follows:

$$\gamma_{wi} = \frac{3n' + 1}{4n'}\gamma_{wa} \tag{5}$$

where n' is defined as

$$n' = \frac{d\ln(\tau_w)}{d\ln(\gamma_{wa})}. \tag{6}$$

According to Enzendorfer et al., 1995, the relationship between n and n' could be expressed as

$$n = \frac{n'}{1 - \frac{1}{3n'+1}\frac{dn'}{d(\ln(\tau_w))}} \tag{7}$$

For power-law behavior fluid, $\frac{dn'}{d(\ln(\tau_w))} = 0$, therefore. n= n'.
The consistency index, K could be found by

$$K = \frac{K'}{\left(\frac{3n'+1}{4n'}\right)^{n'}} \tag{8}$$

where K' is the wall shear stress τ_w at $\gamma_{wa} = 1\,s^{-1}$. Finally, the apparent viscosity of the foam at different shear rates could be calculated as:

$$\mu_a = K\gamma_{wi}^{n-1} \tag{9}$$

Fig. 4a shows the log-log plot of γ_{wa} vs. τ_w, and the apparent viscosity of the foam could be given by the equations in Fig. 4b. Based on the measured data, the foam behaves like a shear-thinning fluid.

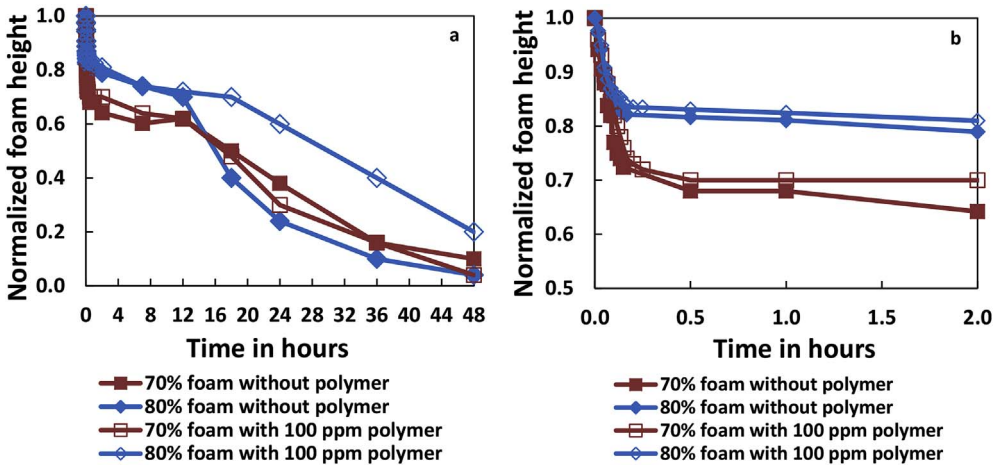

Fig. 3. Normalized foam height (a) for 48 h (b) for the first 2 h.

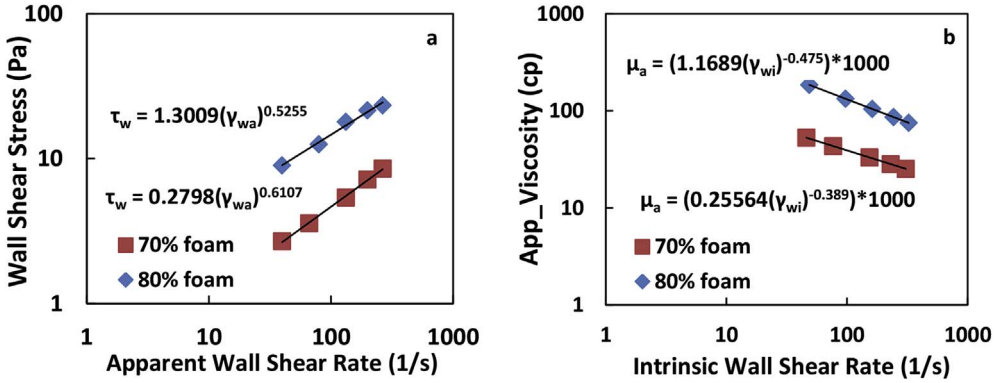

Fig. 4. Foam rheological data (a) wall shear stress and (b) apparent viscosity.

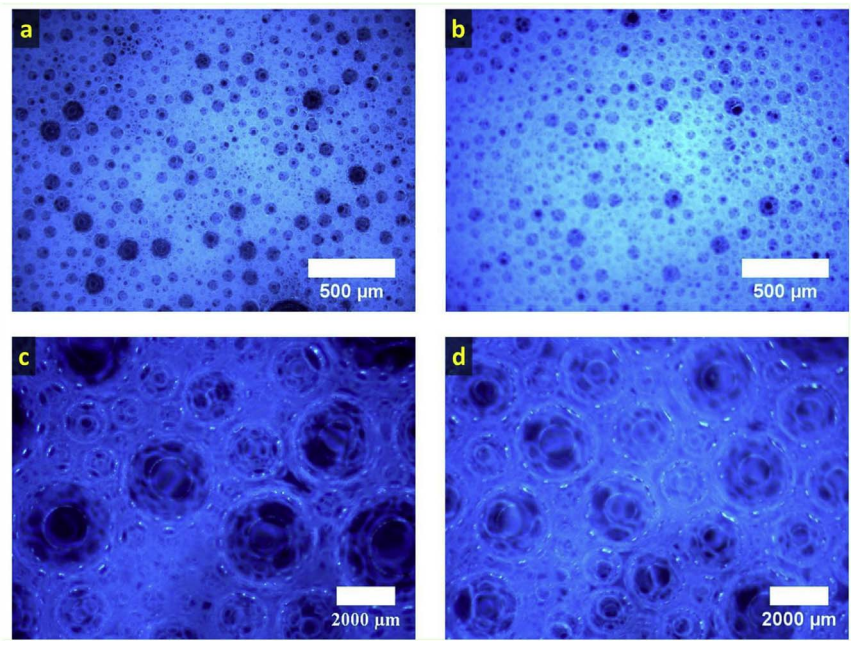

Fig. 5. Foam texture of 70% quality foam at (a,c) $\overline{X}$ = 0.25 and (b,d) $\overline{X}$ = 0.75.

Table 2
Bubble diameter of the foam of different quality in the Hele-Shaw cell.

Foam quality	Bubble diameter (µm) at $\overline{X}$ = 0.25	Bubble diameter (µm) at $\overline{X}$ = 0.75
70%	1258 ± 711	1399 ± 608
80%	966 ± 539	1149 ± 585

3.3. Characterization of foam-flow in Hele-Shaw cell

3.3.1. Foam texture analysis

Foam texture or the bubble size distribution is one of the most important parameters that governs the foam rheology in both bulk and in porous media. Several studies have shown that smaller bubbles (often referred to as 'finer bubbles') lead to larger flow resistance during flow through porous media (Friedmann and Jensen, 1986; Kovscek and Radke, 1994). Proppant-free foam was injected into the Hele-Shaw cell at two different qualities (70% and 80%) and the flow was stopped once the cell was completely filled with foam. Then, optical micrographs of the foams were captured at dimensionless positions, $\overline{X}$ = 0.25 and $\overline{X}$ = 0.75. Fig. 5 shows the bubble texture for 70% foam. Fig. 5a,c shows the snapshots at $\overline{X}$ = 0.25, and Fig. 5b,d shows the snapshots at $\overline{X}$ = 0.75. The bubble size was quantified using image analysis (Fiji software) and is listed in Table 2. For 70% quality, the bubble diameters were 1258 ± 711 µm and 1399 ± 608 µm at $\overline{X}$ = 0.25 and $\overline{X}$ = 0.75, respectively. Only a small change in bubble texture was observed between the inlet and the outlet. The pressure change within the cell does not change the bubble texture significantly because the pressure drop across the cell is low (as discussed in the next section). Similarly, foam of 80% quality was injected into the cell and bubble texture was studied. Fig. 6a, c and Fig. 6b,d shows the bubble texture at $\overline{X}$ = 0.25 and $\overline{X}$ = 0.75, respectively. The corresponding bubble diameters were found to be 966 ± 539 µm and 1149 ± 585 µm. Note that, similar to the 70% quality case, the change in bubble texture was small. Also, the bubble size in 70% case was larger than that of 80% case indicating relatively weaker foam.

3.3.2. Pressure drop

In this study, proppant-free foams of different qualities were injected and steady-state pressure drop across the cell was measured

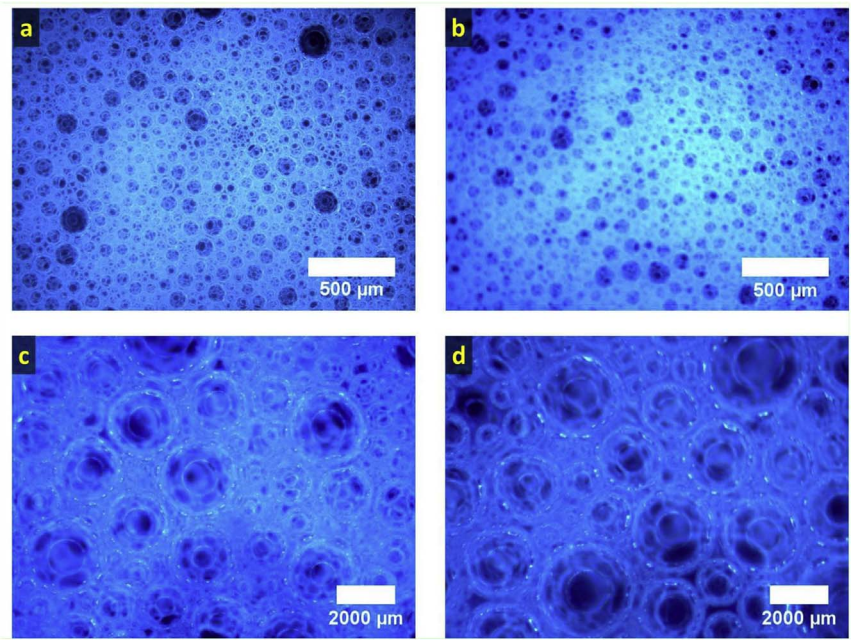

Fig. 6. Foam texture of 80% quality foam at (a,c) $\overline{X}$ = 0.25 and (b,d) $\overline{X}$ = 0.75.

Table 3
Pressure drop for foam flow without proppants.

Foam Quality	Injection Rate (ml/min)	Nominal Shear Rate (1/s)	Pressure Drop (psi)
70%	250	42	0.3
70%	500	84	0.5
70%	840	140	0.6
80%	250	42	0.8
80%	500	84	1.5
80%	840	140	2.0

(including those in valves and fittings). Table 3 lists the pressure drops. The observed pressure drop across the cell was less than 0.6 psi and 2 psi for 70% and 80% cases, respectively. Since these pressure drop values are low, the absolute pressure did not change substantially across the slot and thus its effect on foam rheology (Holt et al., 1996) was small.

3.3.3. Injection rate validation

The injection pressure, in principle, can affect the mass flow rate (for a specified volumetric flow rate) because the foam is compressible. Since the pressure drops (Table 3) were low in the present study, the injection rates were almost constant during the floods. To further validate this, foam was injected into the cell at two different qualities at 250 ml/min injection rate (equivalent to 42 s^{-1} shear rate) and the foam front was tracked using a video camera. Fig. 7a and b shows the foam fronts at several times for 70% and 80% quality, respectively. The x- and z-axis are the normalized positions in x and z directions. The volume of foam injection was calculated by the area coverage of the slot using Fiji software, and the data were plotted in Fig. 8. The injection rates were found to be 256 ml/min and 249 ml/min for 70% and 80% cases, respectively. These rates were very close to the nominal injection rate of the pump, i.e., 250 ml/min. This shows that the pump could inject the foam at specified rates. The same was validated for the other injection rates used in the present study.

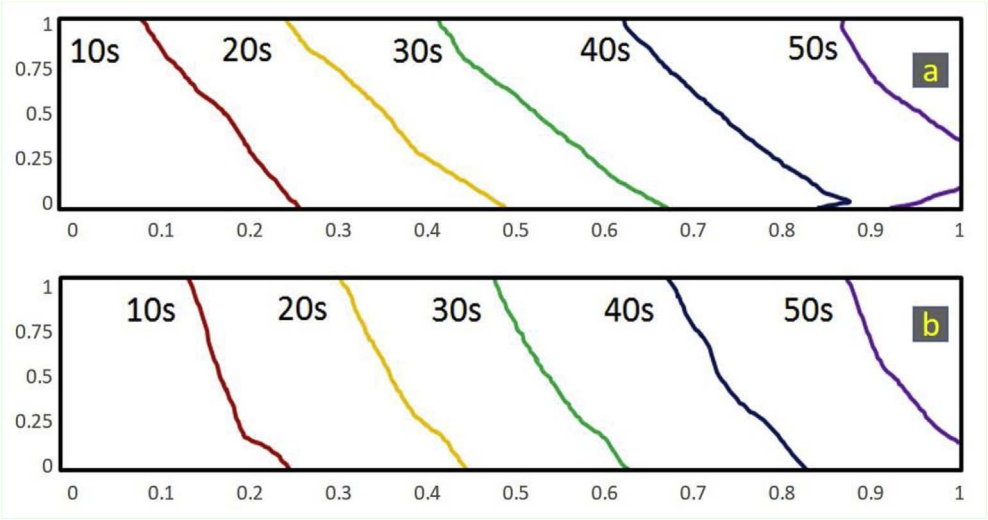

Fig. 7. Foam front at different injection times for (a) 70% quality foam, (b) 80% quality foam.

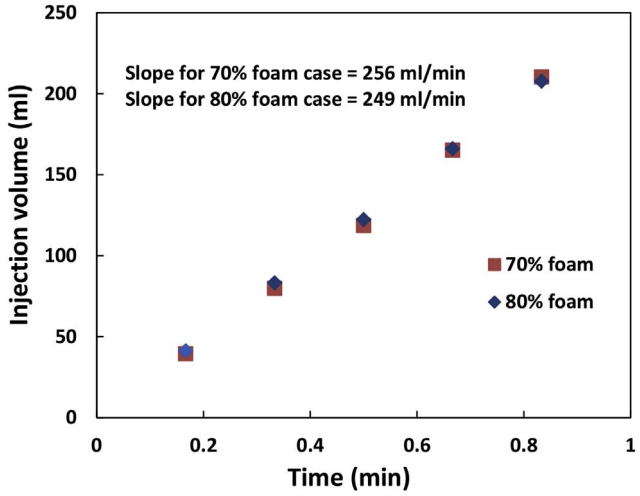

Fig. 8. Injection volume (based on image analysis of foam coverage in the Hele-Shaw cell) as a function of time.

3.4. Proppant transport

In this study, 80% quality foam is considered as the base case, and a typical proppant transport pattern in 80% quality foam is shown in Fig. 9. Four zones are generally observed in the slot during proppant transport in foam: a thin proppant-lean zone at the top due to proppant settling, a proppant-rich foam zone in the middle, a foam-rich (proppant lean) zone towards the bottom and a thin settled-proppant bed zone at the very bottom of the fracture. The bottom foam-rich (proppant lean) zone tends to migrate upward in the form of fingers into the proppant-rich foam zone due to gravitational forces. As the fingers move upward, the proppant surrounding them are pushed away similar to immiscible displacements. The proppant on top of the fingers could move upward, and the proppant along the two sides of the fingers would settle faster compared to those in the finger-free zone. There are possibly two causes for finger generation. First, a foam-rich layer at the bottom is formed due to liquid separation at the inlet. Second, as proppants drop out of the slurry to form a proppant bed at the bottom of the fracture slot, the excess foam would merge to form fingers. This phenomenon could generate pillars of proppant-free zones (Gomaa et al., 2016).

Proppant trajectories were tracked in a video analysis software, and their velocity was calculated. The tracked proppants were chosen in the center region of the slot (dashed line region in Fig. 9) to avoid entrance and outlet effects. In all cases, the slurry at the bottom of the slot moved faster than those in the top and middle section. Therefore, the proppants were selected from the middle to the bottom of the slot to better understand the velocity variation due to sampling positions. Additionally, proppants around the fingers were avoided because their velocity could vary significantly due to the movement of the fingers. Fig. 10 shows typical movements of a tracked proppant in horizontal (x) and downward vertical (z) directions, and it shows that both proppant x and z velocities are approximately constant with respect to time. In all 80% foam cases, foam significantly decreased gravity settling of proppants compared to that of water. Unlike a continuum non-Newtonian fluid, the force exerted on the proppant by the foam could be categorized into two components: a drag force due to the bulk movement of the fluid and an elastic force due to foam compressibility and lamella movement (Jing et al., 2016). Therefore, foam is more effective than continuum viscous fluids in terms of carrying proppants.

3.5. Effect of foam quality

As the foam quality increases, the viscosity of the foam increases (as shown in Fig. 4) and the lamella structure changes. Both affect proppant settling. When foam is dry, the liquid lamellas are better defined, and proppant could be nicely trapped by these microstructures with negligible settling. When foam is wet, the liquid portions in between the gas bubbles get bigger, some of the proppants do not interact with interfaces and settle faster. Fig. 11 shows the proppant distribution at the end of injection for cases 1, 13, 9 and 15. Cases 1 and 13 were conducted at a low shear rate, but have the same parameters except for the foam quality. Cases 9 and 15 were conducted at a high shear rate, with the same parameters except for the foam quality. For dry foam (80% quality) cases (cases 1 and 9), very little proppant settled down and most of the proppant flowed out of the slot. For wet foam (70% quality) cases (case 13 and 15), proppant settled very quickly and formed a proppant bed at the inlet entrance, which is very similar to that of slickwater slurry (Woodworth and Miskimins, 2007). Additionally, clear foaming solution accumulated near the outlet, which is partly due to severe liquid draining at the outlet well when the foam is wet. The local foam quality was smaller than 70% at the lower section of the slot, which could lead to lower foam viscosity and faster proppant settling.

3.6. Effect of shear rate

Fig. 12 shows the proppant distribution in the fracture slot for cases 1, 5 and 9. All parameters are kept constant except for the shear rate. The slurry was injected from the left in the empty slot filled with air. Two interesting observations were made from Fig. 12. First, more fingers were observed at lower shear rate (case 1). This is because there is more time for fingers to grow. Second, at the lowest shear rate, a small proppant bed forms; there are no proppant beds at the higher shear

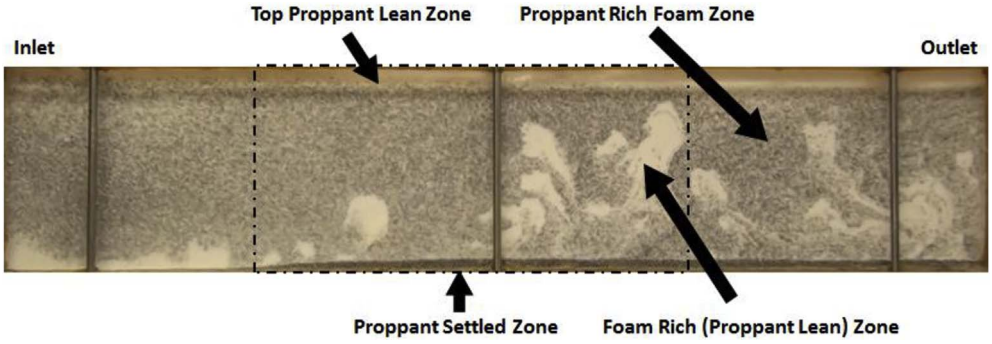

Fig. 9. Typical proppant transport pattern in 80% quality foam.

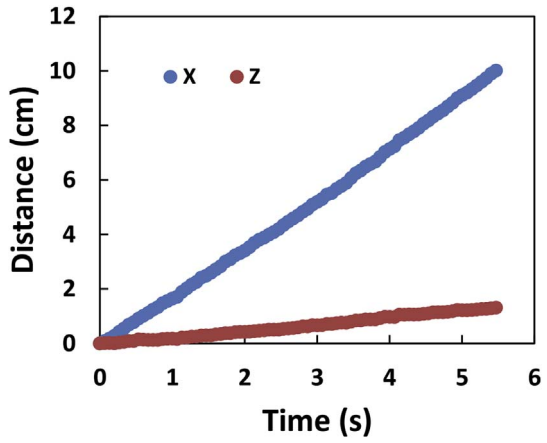

Fig. 10. Proppant movement in 80% quality foam.

rates. There could be two possible reasons for these phenomena. First, as the foam moves faster, proppants have less time to settle before flowing out of the slot. Additionally, greater drag force is exerted on the proppants with faster foam, and this force can mobilize settled proppants and limit the size of the proppant bed. Second, as the fingers move upward, proppants along the two sides of the fingers tend to settle down faster. Therefore, in low shear rate scenario (case 1), the greater size and number of these fingers could result in more settling of proppants and consequently a larger proppant bed.

Fig. 13a and b shows the proppant settling velocity (V_z) and normalized proppant x-velocity (Vx/Vx_Foam), respectively, against the normalized height of the slot for cases 1, 5 and 9. V_x is the x-velocity of the proppant, and Vx_Foam is the nominal x-velocity of the foam (injection rate/cross-sectional area). No data is shown in the upper section of the slot because the proppants seldom settle down when the normalized height is greater than 0.5. Based on all experiments data (including all loading cases), at the same normalized height, the normalized proppant x-velocity gets smaller as the shear rate increases. Generally, the foam moves faster at the bottom of the slot probably due to lower local foam quality; thus the proppants also flow a little faster at the bottom. In the upper section of the slot, Vz is almost zero and proppants do not settle. The proppants are carried by the foam lamella very effectively. In the lower section of the slot, most proppants settle (negative Vz). In addition, proppant settles faster as the shear rate decreases as shown in Fig. 13b. For some proppants, the settling velocity is slightly positive, which means some proppants move slightly upward. Proppants moved upwards due to the complex flow pattern created by the foam fingers and the foam drainage process. To illustrate this, a few snapshots are shown in Fig. 14. As the liquid phase drains down, the foam bubbles move upward and could drag the proppant upward. Fig. 15a shows V_z as a function of the normalized proppant x-velocity. It could be observed when the normalized proppant x-velocity is less than

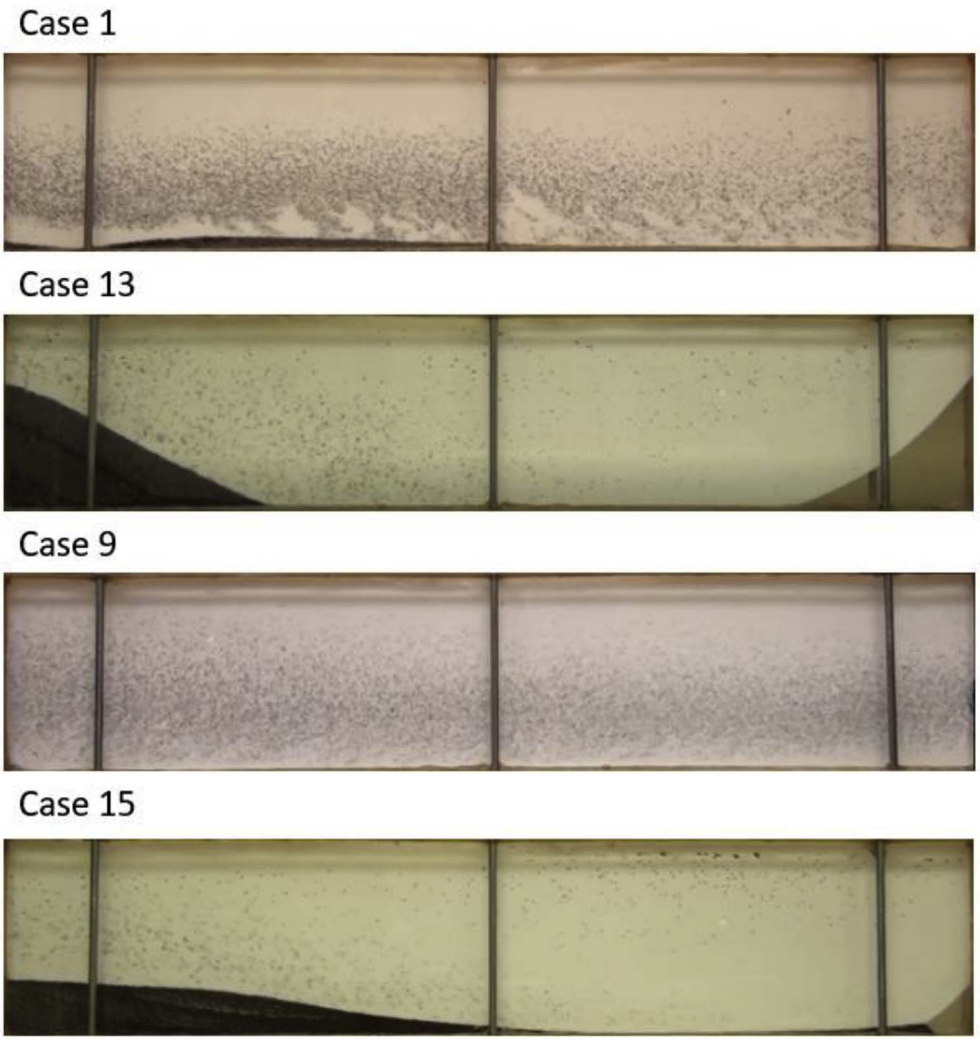

Fig. 11. Effect of foam quality for cases with 2.5 vol% proppant loading: low shear rates (Case 1: 42 s^{-1} in 80% foam vs. Case 13: 42 s^{-1} in 70% foam), high shear rates (Case 9: 140 s^{-1} in 80% foam vs. Case 15: 140 s^{-1} in 70% foam).

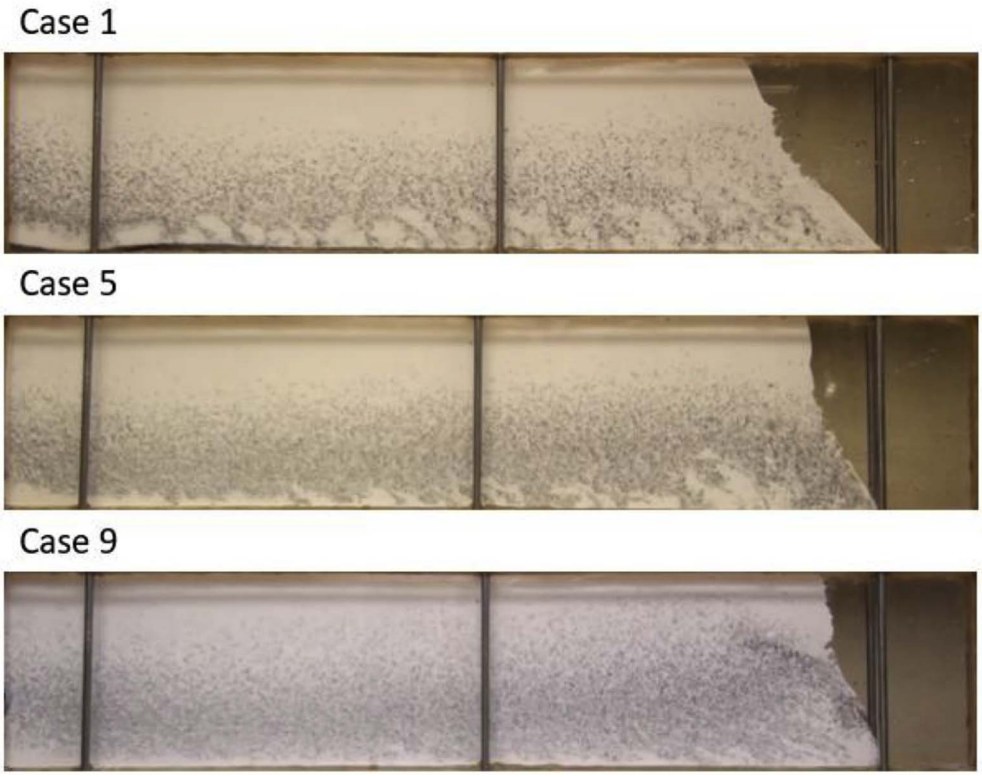

Fig. 12. Proppant settling in 80% foam with 2.5 vol% proppant; Case 1: 42 s^{-1} shear rate, Case 5: 84 s^{-1} shear rate, and Case 9: 140 s^{-1} shear rate.

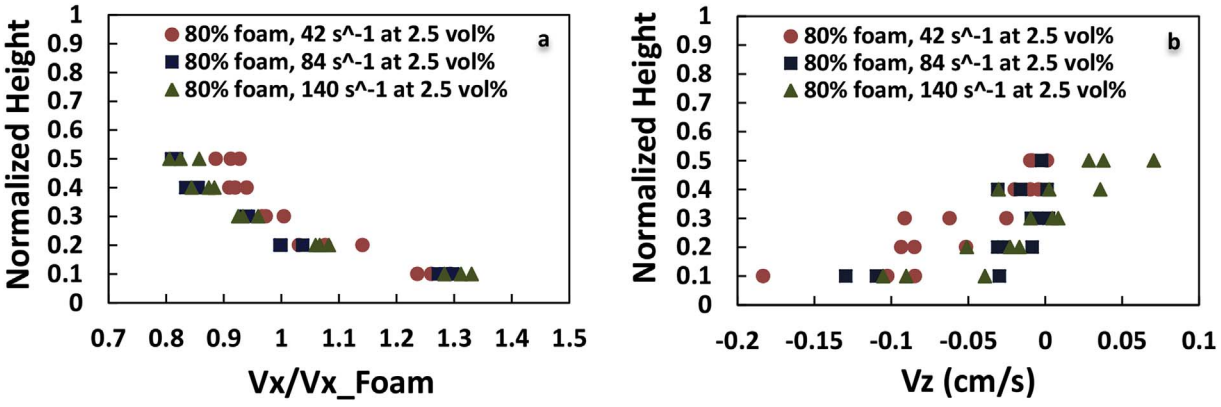

Fig. 13. Effect of nominal shear rate on proppant settling velocity in 80% foam with 2.5 vol% proppant (a) normalized horizontal velocity, (b) vertical velocity.

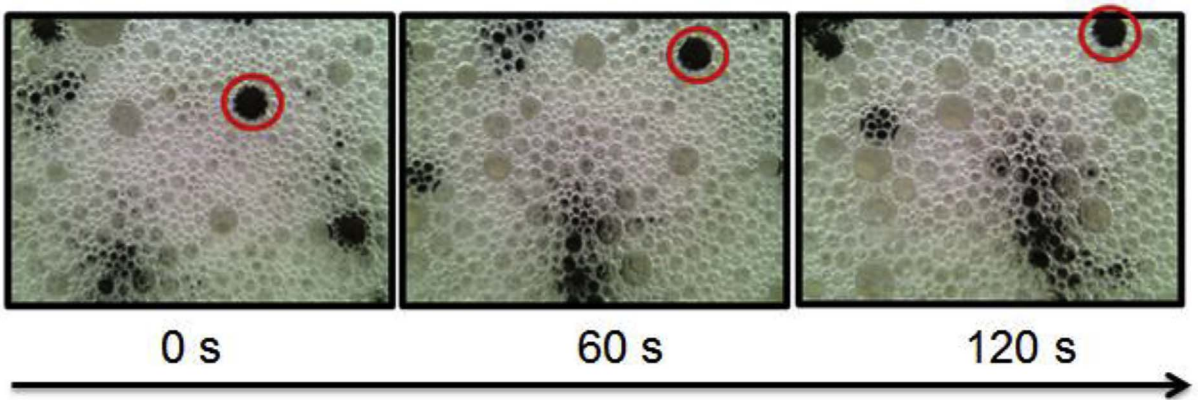

Fig. 14. Upward proppant movement due to liquid drainage.

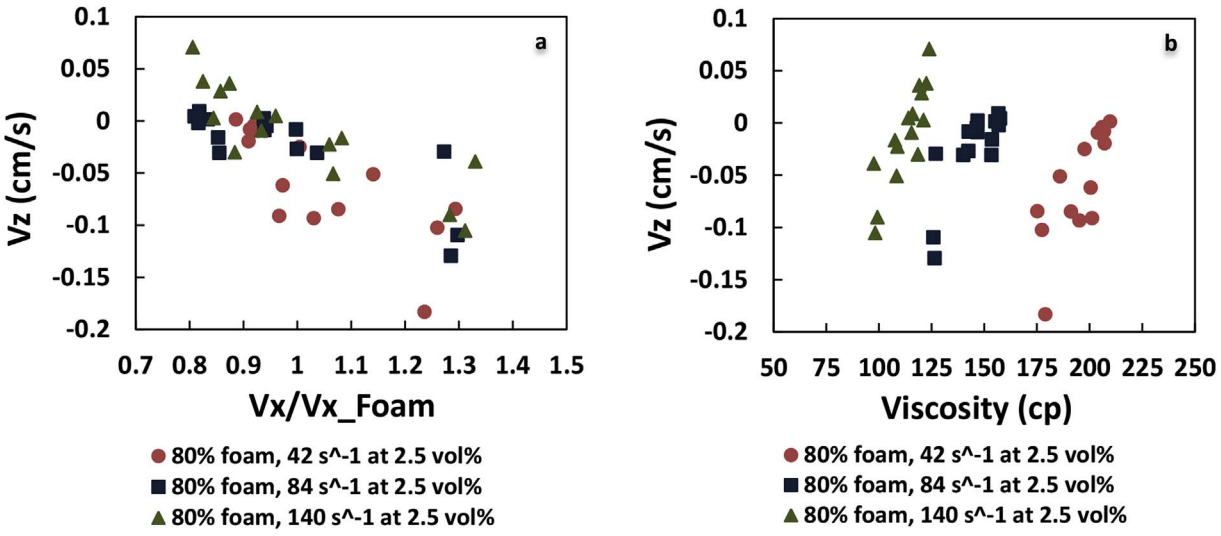

Fig. 15. Effect of nominal shear rate on proppant settling velocity in 80% foam with 2.5 vol% proppant (a) Vz vs. normalized Vx, (b) Vz vs. nominal foam viscosity.

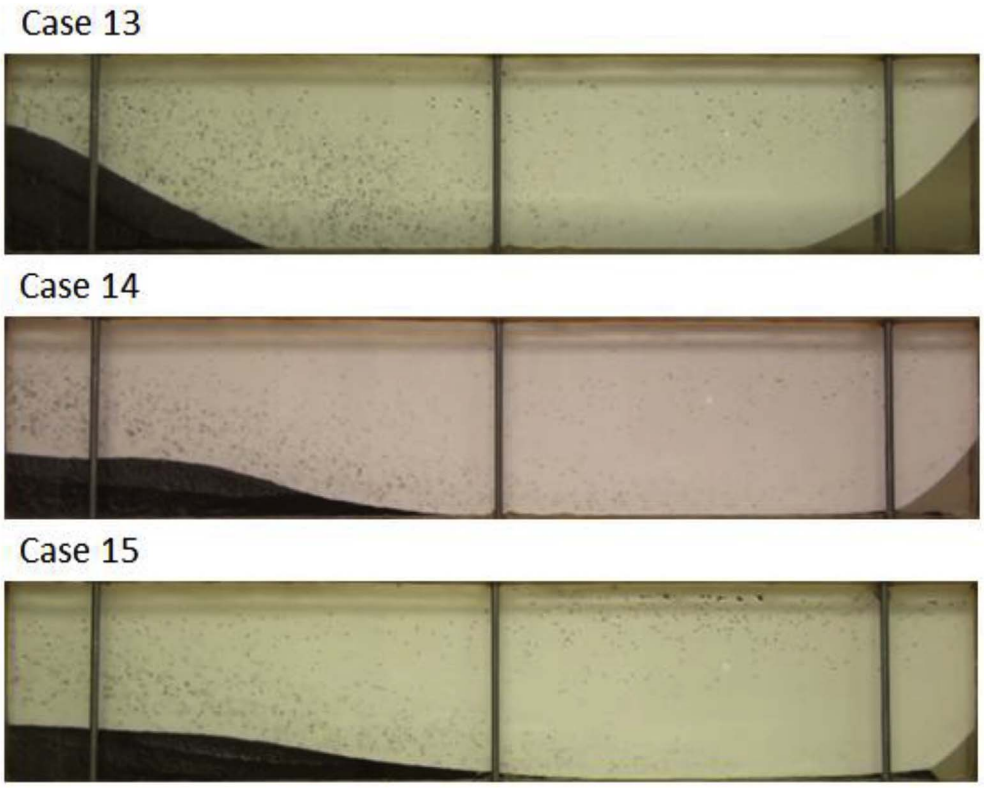

Fig. 16. Proppant settling in 70% foam with 2.5 vol% proppant; Case 13: 42 s^{-1} shear rate, Case 14: 84 s^{-1} shear rate, and Case 15: 140 s^{-1} shear rate.

0.9, proppants settle very slowly or even move upward. If we assume the proppant x-velocity is equal to the local foam x-velocity, then we could calculate the local apparent viscosity with the correlations shown in Fig. 4. In Fig. 15b, it indicates proppant settles slower if the nominal shear rate is higher, and there are two possible mechanisms for this phenomena. First, a faster foam limits the growth of the foam fingers which could lead to greater settling to adjacent proppant; second, the foam quality is more uniform in a faster (or higher shear rate) foam due to less time for drainage process.

Fig. 16 shows the proppant distribution at the end of injection for 70% quality foam cases 13–15. As shear rate increases, the proppant bed gets shorter (in height) and longer. The surfactant water drains slowly towards the bottom of the slot and lowers the foam quality. Proppants settle in a way similar to slick water at the bottom. Fig. 17 shows the vertical and horizontal velocities of some of the proppants not yet settled into the proppant bed. The settling velocity ranges from 0.8 cm/s to 2.1 cm/s, and these values are significantly larger than those in 80% foam cases. It was difficult to measure the velocity value against normalized height because proppant bed formed very quickly during the experiments.

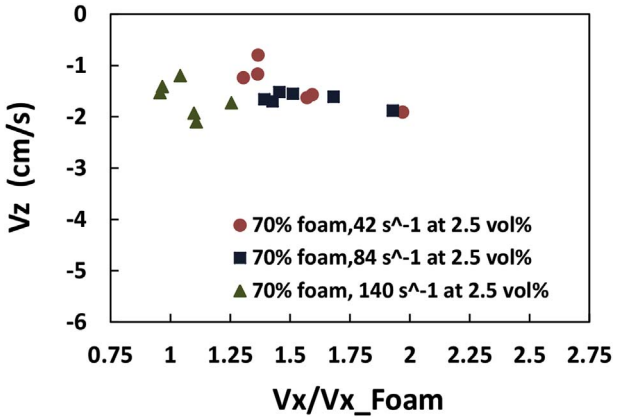

Fig. 17. Effect of nominal shear rate on proppant settling velocity in 70% foam with 2.5 vol% proppant.

3.7. Effect of proppant loading

Fig. 18a and b shows the proppant settling velocity (Vz) and normalized proppant horizontal velocity against normalized height for cases 5 to 8, respectively. Proppant loading is varied keeping other parameters constant. According to Fig. 18a, the proppant loading does not have a significant impact on the normalized proppant x-velocity profile. According to Fig. 18b, in the middle of the slot, the settling velocity is almost zero; there is no settling of proppants. In the bottom of the slot, the settling velocity magnitude and its variations are larger for the dilute proppant loading cases (2.5 and 5.0 vol%) than those of dense cases (7.5 and 10.0 vol%). This indicates that as proppant loading increases (below a threshold value above which proppants significantly damage the microstructure of the foam), the foam microstructure and adjacent proppants hinder proppant settling. Fig. 19a shows V_z as a function of the normalized proppant x-velocity. It could be observed in Fig. 19a, as the normalized proppant x-velocity increases, proppant settles faster with a larger variation in settling velocity magnitude. According to Fig. 19b, at the same apparent foam viscosity, proppant settles slower with a smaller variation in settling velocity magnitude as the loading increases. Based on these observations, at typical field proppant loading range, the foam could effectively carry the proppants at 80% quality.

Fig. 20 shows the proppant distribution at the end of injection for 70% foam cases 15–17. As proppant loading increases, the proppant bed height grows. Fig. 21 shows the velocity data for these three cases, and the existence of a big proppant bed leads to a larger value of Vx/Vx_Foam as less cross-sectional area is available for proppant and foam flow. The magnitude of settling Vz velocities are large (1-5 cm/s) compared to those in 80% quality foam cases (0.05 cm/s). Proppants settle slower when the loading increases.Fig. 22 compares the settling velocity for experimental proppant particles with the theoretical Stokes settling velocity. The symbols represent the experimental data. Velocities are directly measured; corresponding viscosities are estimated from the shear rate associated with the local foam velocity (which is

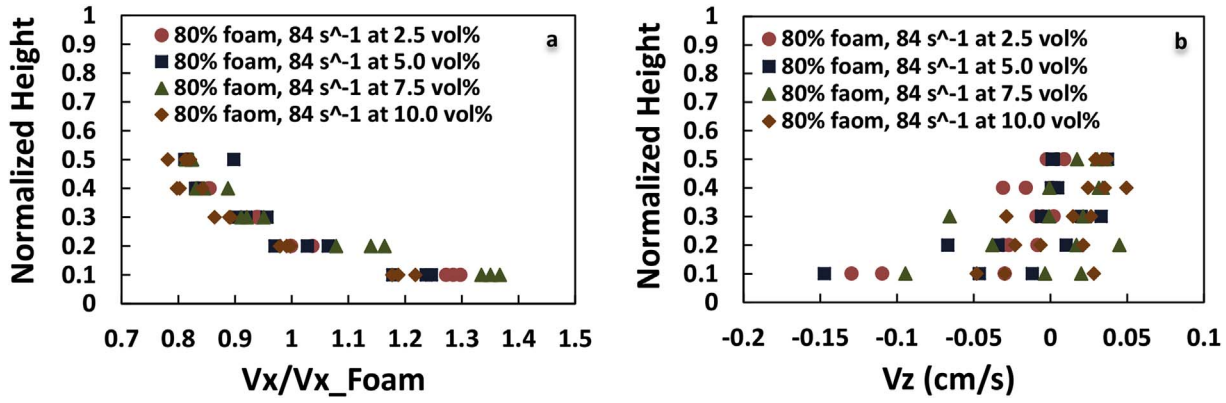

Fig. 18. Effect of proppant loading on proppant settling velocity in 80% foam at 84 s^{-1} (a) horizontal velocity (b) vertical velocity as a function of vertical position.

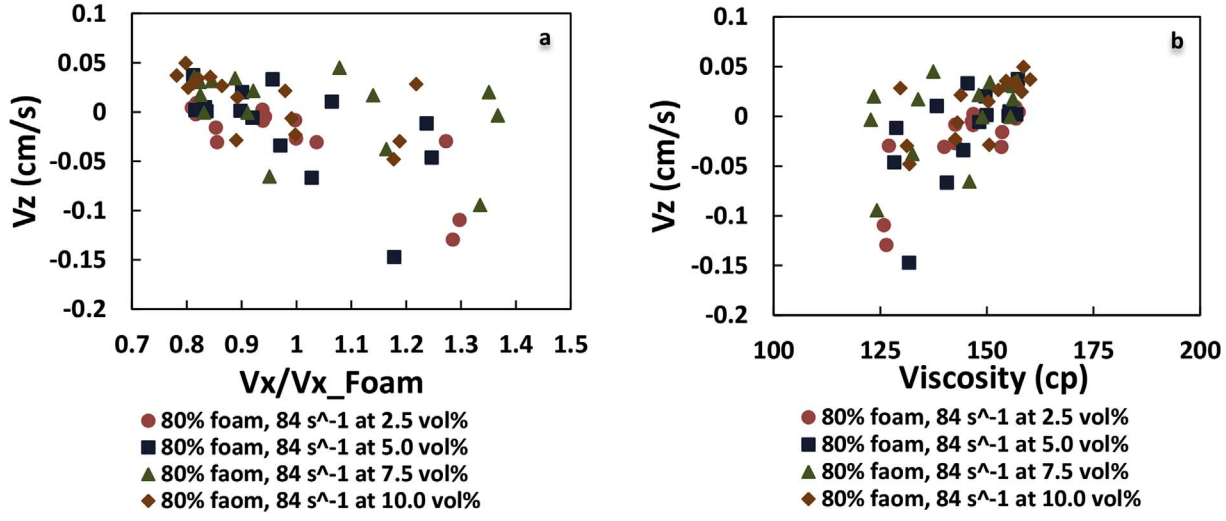

Fig. 19. Effect of proppant loading on proppant settling velocity in 80% foam at 84 s^{-1} (a) Vz vs. normalized Vx, (b) Vz vs. nominal foam viscosity.

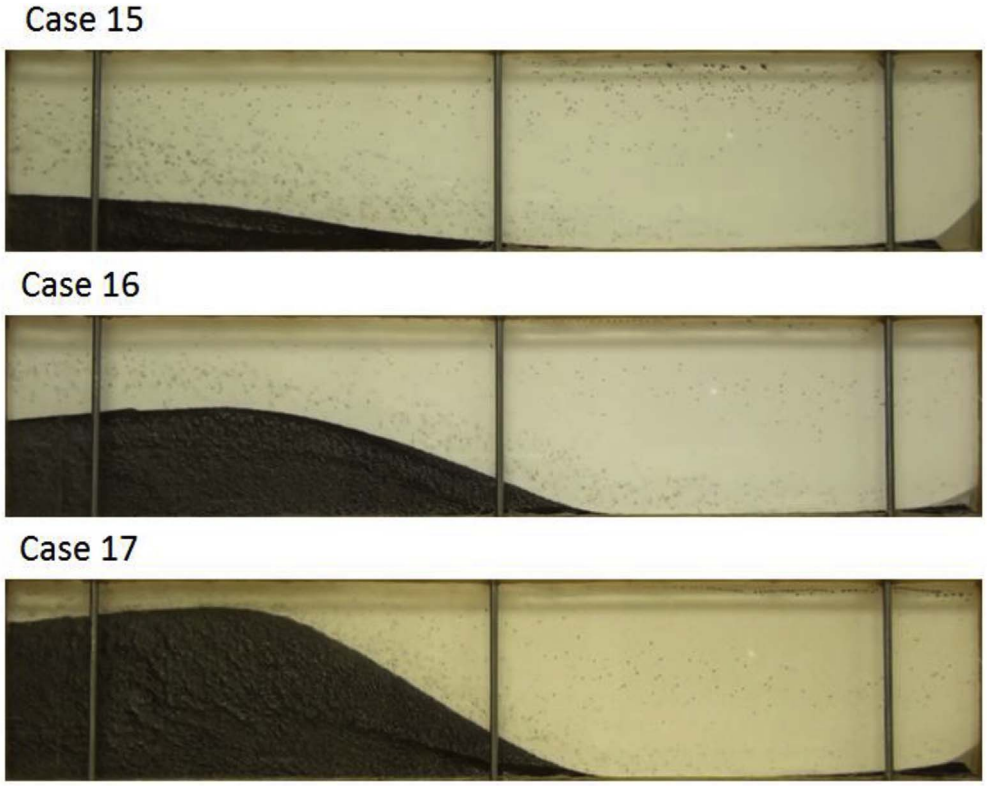

Fig. 20. Comparison of proppant loading for 70% foam cases at 140 s^{-1} shear rate; Case 15: 2.5 vol%, Case 16: 5.0 vol%, and Case 17: 7.5 vol%.

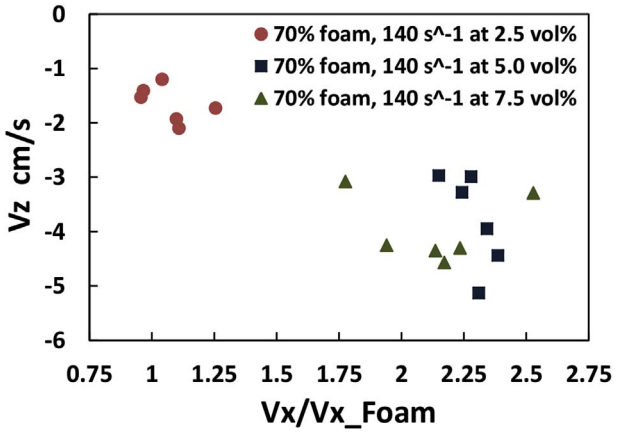

Fig. 21. Effect of proppant loading on proppant settling velocity in 70% foam at 140 s^{-1}: Vz vs. normalized Vx.

approximated by the Vx of the proppant being studied). The red and dashed black curves represent the velocity estimated from Stokes equation, assuming that the proppant diameter is 600 μm (average size for 20-40 mesh) and the density of 80% and 70% quality foams, respectively. Note that the density difference of the two foams does not make a significant difference in the proppant settling velocity. The green dashed curve represents the Stokes velocity for the smallest proppant in the 20-40 mesh in 70% foam and the blue dashed curve for the largest proppant in the 20-40 mesh. It could be observed that all the experimental proppant velocities (the magnitudes) in the 80% foam are very small (mostly less than 0.1 cm/s); these velocities are smaller than the calculated Stokes velocity for the average proppant in 80% foam; they do not follow Stokes law. However, the proppants in 70% foam do follow the Stokes law. This is because in dry 80% foams, a proppant is typically trapped between a set of bubbles, primarily moves with this set of bubbles with little vertical settling, and does not experience the effective viscosity of the foam. However, in 70% foam, proppants settle in the liquid between the bubbles while being hindered by many interfaces, and experience the effective viscosity of the foam.

$$Vz = \frac{d^2 g \Delta\rho}{18\mu}, \tag{10}$$

4. Conclusions

In this work, proppant transport in foam-based fracturing fluid is visualized in a laboratory-scale fracture slot. Effects of parameters like foam quality, proppant loading, and injection rate are systematically investigated. This study is conducted at a low pressure; for reservoir conditions one needs to simulate the foam flow based on the transport properties observed here. The following conclusions are reached in this work.

- Dry foams (80% quality) can carry proppants between lamellas with little vertical settling. Proppants are not carried very well in wet foams (70% quality); they settle and form a proppant bed near the fracture entrance.
- In dry foams, settling velocity of proppants is almost zero in the middle of the fractures. Proppants settle with a very low velocity only at the bottom of the fractures. As the shear rate and the proppant loading increase, the proppant settles slower.
- Complex flow patterns are developed in dry foams due to protrusion of foam fingers into proppant laden foam.
- In wet foams, the surfactant solution cannot carry proppants because of a low viscosity and a proppant bed forms at the fracture entrance, similar to those in slickwater. The height of the proppant bed decreases as the shear rate increases and the proppant loading decreases.

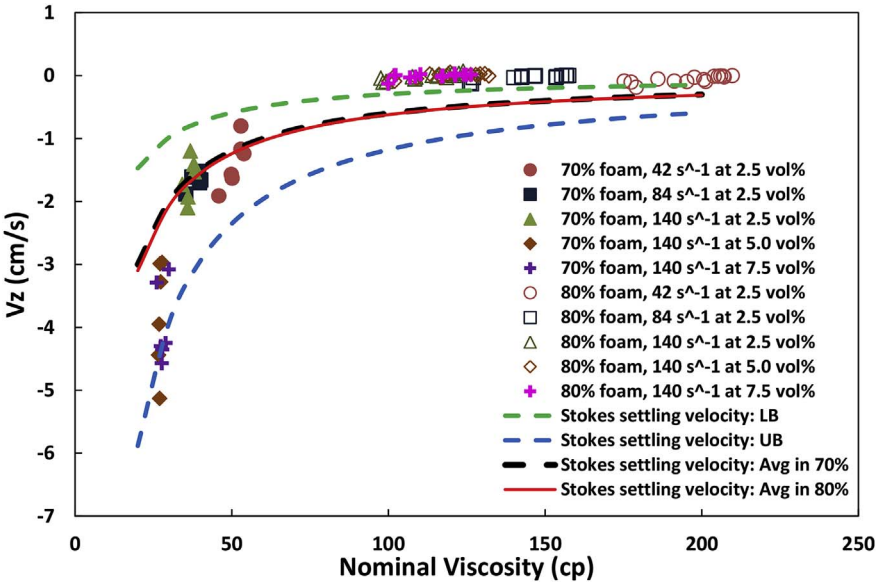

Fig. 22. Comparison of vertical settling velocity of proppant particles with those from Stokes equation; velocity is shown for average particle size in 70% and 80% foams as well as the velocity for the smallest particle (LB) and the largest particle (UB).

Acknowledgements

The authors would like to thank Statoil for a fellowship for Songyang Tong.

Nomenclature

w	slot width, m
h	slot height, m
d	diameter of testing tube, m
L	length of testing tube, m
q	injection rate, m^3/s
γ	shear rate, 1/s
μ	viscosity, cp
ΔP	pressure difference, pa
τ	stress, pa
n	power law index, no unit
K	consistency index, Ns^n/m^2

References

Andrianov, A., Farajzadeh, R., Mahmoodi Nick, M., Talanana, M., Zitha, P.L.J., 2012. Immiscible foam for enhancing oil recovery: bulk and porous media experiments. Ind. Eng. Chem. Res. 51, 2214–2226. https://doi.org/10.1021/ie201872v.

Barati, R., Liang, J.-T., 2014. A review of fracturing fluid systems used for hydraulic fracturing of oil and gas wells. J. Appl. Polym. Sci. 131 n/a-n/a. https://doi.org/10.1002/app.40735.

Doorwar, S., Mohanty, K.K., 2011. Viscous fingering during non-thermal heavy oil recovery. In: SPE Annual Technical Conference and Exhibition. 30 Oct- 2 Nov, Denver, Colorado, USA SPE-146841. https://doi.org/10.2118/146841-MS.

Enzendorfer, C., Harris, R.A., Valko, P., Economides, M.J., Fokker, P.A., Davies, D.D., 1995. Pipe viscometry of foams. J. Rheol. 39, 345–358.

Friedmann, F., Jensen, J.A., 1986. Some parameters influencing the formation and propagation of foams in porous media. In: Presented at the SPE California Regional Meeting, Society of Petroleum Engineers. https://doi.org/10.2118/15087-MS.

Gaurav, A., Dao, E.K., Mohanty, K.K., 2012. Evaluation of ultra-light-weight proppants for shale fracturing. J. Petrol. Sci. Eng. 92–93, 82–88. https://doi.org/10.1016/j.petrol.2012.06.010.

Gomaa, A.M., Hudson, H., Nelson, S., Brannon, H., 2016. Improving fracture conductivity by developing and optimizing channels within the fracture geometry: CFD study. In: SPE International Conference and Exhibition on Formation Damage Control. 24–26 Feb, Lafayette, Louisiana, USA SPE-178982. https://doi.org/10.2118/178982-MS.

Gu, M., Mohanty, K.K., 2015. Rheology of polymer-free foam fracturing fluids. J. Petrol. Sci. Eng. 134, 87–96. https://doi.org/10.1016/j.petrol.2015.07.018.

Gu, M., Mohanty, K.K., 2014. Effect of foam quality on effectiveness of hydraulic fracturing in shales. Int. J. Rock Mech. Min. Sci. 70, 273–285. https://doi.org/10.1016/j.ijrmms.2014.05.013.

Harris, P.C., 1995. A comparison of mixed gas foams with N2 and C02 foam fracturing fluids on a flow loop viscometer. SPE Prod. Facil. 10, 197–203. https://doi.org/10.2118/20642-PA.

Harris, P.C., 1989. Effects of texture on rheology of foam fracturing fluids. SPE Prod. Eng. 4, 249–257. https://doi.org/10.2118/14257-PA.

Harris, P.C., Reidenbach, V.G., 1987. High-temperature rheological study of foam fracturing fluids. J. Petrol. Technol. 39, 613–619. https://doi.org/10.2118/13177-PA.

Holt, T., Vassenden, F., Svorstol, I., 1996. Effects of pressure on foam stability; implications for foam screening. In: Presented at the SPE/DOE Improved Oil Recovery Symposium Society of Petroleum Engineers. https://doi.org/10.2118/35398-MS.

Jing, Z., Wang, S., Wang, Z., 2016. Detailed structural and mechanical response of wet foam to the settling particle. Langmuir 32, 2419–2427. https://doi.org/10.1021/acs.langmuir.6b00281.

Kadhim, D., Imqam, A., Dunn-Norman, S., 2017. Ceramic proppant transport and placement in heterogeneous fracture systems. In: SPE/AAPG/SEG Unconventional Resources Technology Conference. 24–26 Jul, Austin, Texas, USA URTEC-2697613-MS.

Kern, L.R., Perkins, T.K., Wyant, R.E., 1959. The mechanics of sand movement in fracturing. J. Petrol. Technol. 11, 55–57. https://doi.org/10.2118/1108-G.

Kong, X., McAndrew, J., Cisternas, P., 2016. CFD study of using foam fracturing fluid for proppant transport in hydraulic fractures. In: Abu Dhabi International Petroleum Exhibition & Conference. 7–10 Nov, Abu Dhabi UAE, SPE-183549-MS. https://doi.org/10.2118/183549-MS.

Kovscek, A.R., Radke, C.J., 1994. Fundamentals of Foam Transport in Porous Media, in: Foams: Fundamentals and Applications in the Petroleum Industry, Advances in Chemistry. American Chemical Society, pp. 115–163. https://doi.org/10.1021/ba-1994-0242.ch003.

Liu, Y., Sharma, M.M., 2005. Effect of fracture width and fluid rheology on proppant settling and retardation: an experimental study. In: SPE Annual Technical Conference and Exhibition. 9–12 Oct, Dallas, Texas, USA SPE-96208. https://doi.org/10.2118/96208-MS.

Malhotra, S., Lehman, E.R., Sharma, M.M., 2014. Proppant placement using alternate-slug fracturing. SPE J. 19, 974–985. https://doi.org/10.2118/163851-PA.

McAndrew, J., Cisternas, P., Pruvot, A., Kong, X., Tong, S., 2017. Water consumption and proppant transport aspects of foam fracturing fluids. In: SPE/AAPG/SEG Unconventional Resources Technology Conference. 24–26 Jul, Austin, Texas, USA URTEC-2671549-MS.

Mohanty, K.K., Tong, S., Miller, C., Honarpour, M.M., Turek, E., Peck, D.D., 2017. Improved hydrocarbon recovery using mixtures of energizing chemicals in unconventional reservoirs. In: SPE Annual Technical Conference and Exhibition. Society of Petroleum Engineers, 9–11 Oct, San Antonio, Texas, USA SPE-187240-MS. https://doi.org/10.2118/187240-MS.

Ouyang, L., Yango, T., Zhu, D., Hill, A.D., 2012. Theoretical and experimental modeling of residual gel filter-cake displacement in propped fractures. SPE Prod. Oper. 27, 363–370. https://doi.org/10.2118/147692-PA.

Reidenbach, V.G., Harris, P.C., Lee, Y.N., Lord, D.L., 1986. Rheological study of foam fracturing fluids using nitrogen and carbon dioxide. SPE Prod. Eng. 1, 31–41. https://doi.org/10.2118/12026-PA.

Ribeiro, L.H., Sharma, M.M., 2012. Multiphase fluid-loss properties and return permeability of energized fracturing fluids. SPE Prod. Oper. 27, 265–277. https://doi.org/10.2118/139622-PA.

Rickards, A.R., Brannon, H.D., Wood, W.D., 2006. High strength, ultralightweight proppant lends new dimensions to hydraulic fracturing applications. SPE Prod. Oper. 21, 212–221. https://doi.org/10.2118/84308-PA.

Singh, R., Mohanty, K.K., 2017. Foam flow in a layered, heterogeneous porous medium: a visualization study. Fuel 197, 58–69. https://doi.org/10.1016/j.fuel.2017.02.019.
Singh, R., Mohanty, K.K., 2016. Foams with wettability-altering capabilities for oil-wet carbonates: a synergistic approach. SPE J. 21, 1126–1139. https://doi.org/10.2118/175027-PA.
Tong, S., Mohanty, K.K., 2016. Proppant transport study in fractures with intersections. Fuel 181, 463–477.
Vikingstad, A.K., Skauge, A., Høiland, H., Aarra, M., 2005. Foam–oil interactions analyzed by static foam tests. Colloid. Surface. Physicochem. Eng. Aspect. 260, 189–198.
Warpinski, N.R., Mayerhofer, M.J., Vincent, M.C., Cipolla, C.L., Lolon, E.P., 2009. Stimulating unconventional reservoirs: maximizing network growth while optimizing fracture conductivity. J. Can. Petrol. Technol. 48, 39–51. https://doi.org/10.2118/114173-PA.
Woodworth, T.R., Miskimins, J.L., 2007. Extrapolation of laboratory proppant placement behavior to the field in slickwater fracturing applications. In: SPE Hydraulic Fracturing Technology Conference. 29–31 Jan, College Station, Texas, USA, SPE-106089-MS. https://doi.org/10.2118/106089-MS.
Xu, K., Zhu, P., Colon, T., Huh, C., Balhoff, M., 2017. A microfluidic investigation of the synergistic effect of nanoparticles and surfactants in macro-emulsion-based enhanced oil recovery. SPE J. 22, 459–469. https://doi.org/10.2118/179691-PA.
Yang, H., Balhoff, M.T., 2017. Pore-network modeling of particle retention in porous media. AIChE J. 63, 3118–3131. https://doi.org/10.1002/aic.15593.
Yu, W., Huang, S., Wu, K., Sepehrnoori, K., Zhou, W., 2014. Development of a semi-analytical model for simulation of gas production in shale gas reservoirs. In: Unconventional Resources Technology Conference. 25–27 Aug, Denver, Colorado, USA URTEC-2014-1922945. https://doi.org/10.15530/URTEC-2014-1922945.
Zhou, J., Carman, P., Sun, H., Wheeler, R., Brannon, H., Gupta, D.V.S., Starks, R., 2015. Superior proppant placement and fracture conductivity by soft particle fracturing fluid. In: SPE Production and Operations Symposium. 1–5 Mar, Oklahoma City, Oklahoma, USA SPE-173621. https://doi.org/10.2118/173621-MS.